Degradation of polyester coil-coated materials by accelerated weathering investigated by FTIR-ATR chemical imaging and impedance analysis

Deni Jero, Alexander Wärnheim, Nicolas Caussé, Nathalie Lebozec, Nadine Pébère, Dan Persson, Dominique Thierry

Progress in Organic Coatings 199 (2025) 108953

Contents lists available at ScienceDirect

Progress in Organic Coatings

journal homepage: www.elsevier.com/locate/porgcoat

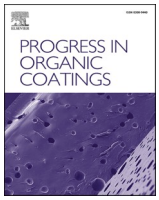

Degradation of polyester coil-coated materials by accelerated weathering investigated by FTIR-ATR chemical imaging and impedance analysis

Deni Jero [a], Alexander Wärnheim [b], Nicolas Caussé [a,*], Nathalie LeBozec [c], Nadine Pébère [a,*], Dan Persson [b], Dominique Thierry [b]

[a] CIRIMAT, Toulouse INP, Université Toulouse 3 Paul Sabatier, CNRS, Université de Toulouse, 4 allée Emile Monso, cedex 4, BP 44362, 31030 Toulouse, France
[b] Research Institutes of Sweden (RISE), Isafjordsgatan 28A, 16407 Kista, Sweden
[c] Institut de la Corrosion/French Corrosion Institute, 220 rue Pierre Rivoalon, 29200 Brest, France

ARTICLE INFO

Keywords:
UV degradation
Depth-resolved FTIR imaging
Water uptake
Plasticization
EIS
Coil-coating

ABSTRACT

In the present study, *ex situ* Fourier transform infrared (FTIR) chemical imaging and *in situ* electrochemical impedance spectroscopy (EIS) were combined to investigate the ageing process of a polyester/melamine coil-coated steel. The samples were first subjected to a QUV accelerated weathering test for 250 h up to 2000 h, followed by immersion in a 0.5 M NaCl solution to assess water uptake and polymer matrix plasticization. FTIR analyses revealed chemical degradation, including chain scission and the formation of polar groups, between 500 h and 2000 h of QUV exposure. Degradation effects were observed throughout the whole topcoat, with more significant degradation occurring near the surface. EIS measurements indicated greater water uptake with increasing QUV exposure, highlighting two regions of water sorption: an initial rapid Fickian diffusion region and a slower non-Fickian region. The time constant (τ) analysis, which was extracted from the EIS data and related to the dielectric manifestation of the glass transition, confirmed polymer matrix plasticization due to water uptake. Despite UV-induced degradation, the polymer maintained effective protective properties, as evidenced by the high low-frequency impedance unaffected by UV exposure or immersion duration (1 week). This methodology successfully identified ageing markers, providing a framework for studying UV degradation mechanisms, water uptake, and polymer mobility in anticorrosion coatings.

1. Introduction

Coil-coatings are organic multilayered materials applied on pre-treated steel or aluminum surfaces, designed to protect metallic surfaces from corrosion in outdoor environments. However, these materials can degrade, leading to blistering, corrosion, and deterioration, particularly in highly deformed areas [1,2]. The degradation of coil-coatings depends on several factors, including surface contamination, the inherent properties of the polymer, and interactions at the metal/polymer interface [3–5]. Environmental conditions, such as humidity and UV radiation, significantly contribute to coating deterioration [6–8]. UV radiation causes photodegradation of the polymer matrix [9] and is frequently assessed *via* standardized tests, such as EN 13523-10. When polymers absorb photons, chemical bonds break, leading to the formation of radicals [10]. The latter can react with oxygen to form oxy- and peroxyradicals, as well as secondary polymer radicals, resulting in chain scission and increased brittleness [7]. Water uptake also plays a crucial role in coating degradation. In particular, water accumulation at the metal/polymer interface can lead to water clustering and blistering [11–15]. It has been shown that water uptake affects the chains' mobility and induces plasticization of the polymer matrix, lowering the glass transition temperature [16–18]. The ingress of water molecules can also induce hydrolysis [19]. The combination of hydrolysis and photolysis can further accelerate coating degradation [19–21].

Due to the complexity of these systems, methods for the rapid evaluation of the performance and stability of coil-coatings are of significant academic and industrial interest. Coating degradation is often assessed by quantifying surface-level changes in color or gloss [20]. However, these methods typically do not provide detailed insights into the specific physical and chemical changes occurring during degradation. Therefore, complementary spectroscopic and microscopic methods are often employed to analyze the surface and bulk properties of coatings [22–27].

Infrared spectroscopy is commonly used to determine and quantify

* Corresponding authors.
E-mail addresses: nicolas.causse@toulouse-inp.fr (N. Caussé), nadine.pebere@ensiacet.fr (N. Pébère).

https://doi.org/10.1016/j.porgcoat.2024.108953
Received 11 September 2024; Received in revised form 16 October 2024; Accepted 19 November 2024
Available online 29 November 2024

chemical changes that occur during both curing and degradation processes [7,27,28]. Additionally, *depth-resolved* infrared spectroscopy has been employed to assess the chemical state within the coating [9,27,29–31]. This is typically achieved by monitoring changes in the infrared spectra that correspond to the chemical degradation of the coating. For example, the formation of degradation products during oxidation in many polymer matrixes can be quantified by observing the growth of the band at approximately 3300 cm^{-1}, which is associated with the formation of –OH groups [20,32]. In polyester/melamine coil-coatings, the loss of crosslinker functionality can be quantified by the decrease in the intensity of the 1550 cm^{-1} band, which is associated with the triazine group in melamine [22,23,26,29].

The water uptake within coil-coatings is typically assessed using gravimetry and electrochemical impedance spectroscopy (EIS). EIS offers several advantages over gravimetry, such as continuous monitoring of water uptake, evaluation of water uptake over short immersion times (within minutes), and *in situ* measurements at temperatures up to 60 °C [33]. Additionally, impedance data allow for the simultaneous study of water uptake, the dielectric manifestation of the glass transition of polymer matrixes [33], and corrosion phenomena. In our recent work, an approach was proposed to study the degradation of polyester coil-coatings by combining the determination of water uptake and its effect on the physical structure of the coating from the dielectric analysis of EIS data. Experiments conducted at room temperature over several months of immersion in a 0.5 M NaCl solution revealed that water uptake affected the physical structure of the organic coating without causing blistering [34]. However, increasing the temperature from 30 °C to 60 °C accelerated the plasticization phenomenon, leading to increased water uptake. At temperatures above 40 °C, the coil-coating exhibited blistering, which was correlated with corrosion at the metal/polymer interface [33]. These studies showed that relevant parameters extracted from impedance spectra can be used to monitor changes in the coating structure under simple ageing conditions such as time and temperature.

The aim of the present work was to combine *ex situ* Fourier transform infrared spectroscopy—attenuated total reflection (FTIR-ATR) and *in situ* EIS to investigate the chemical and physical structure of the same polyester/melamine coil-coated steel, as in our previous works [33,34], but for more complex and representative ageing conditions. Thus, samples were subjected to a QUV accelerated weathering test for durations from 250 h up to 2000 h. FTIR-ATR measurements of the surfaces and *depth-resolved* FTIR were employed to monitor chemical changes in the polymer matrix structure after different exposure times to the weathering test, considering several parameters such as the oxidative index (OI) and the melamine substitution functionality loss (MSFL). EIS measurements were performed at room temperature in a 0.5 M NaCl solution over one week of immersion. Relevant markers of the ageing process were identified and used to analyze water uptake and plasticization of the coating as a function of the QUV exposure time.

2. Experimental

2.1. Materials

The commercial coil-coated material was composed of galvanized steel (hot-dipped galvanized steel with a zinc coating of 275 g m^{-2}) on which a chromium-free primer and a topcoat were deposited, once a titanium-zirconium conversion layer was applied. Both polymer layers were based on polyester (PES) chemistry with thicknesses of 5 μm and 20 μm for the primer and the topcoat, respectively. The used primer was a polyester/melamine/epoxy system with a total pigment volume concentration (PVC) of 18 %, containing phosphates as inhibitive pigments. The topcoat was a polyester/melamine system with a total PVC of 22 %. Before the electrochemical measurements, the samples were dried for 16 h at 60 °C (dry state) to guarantee the same initial state [33,34]. The glass transition temperature (T_g) of the reference dried sample was 21 ± 1 °C [34].

2.2. Accelerated QUVA weathering test

The samples were subjected to an artificial weathering test in a QUV Chamber (from the Q-Panel). The cycle (dry UV irradiation followed by humid condensation) was performed according to a modified EN 13523-10 standard test at a peak irradiance of 1.36 W m^{-2} at 340 nm and a temperature of 80 °C during exposure to UV radiation (4 h), followed by condensation at 40 °C (4 h). One sample was taken after 250 h, 500 h, 1000 h, 1500 h and 2000 h of exposure for characterization *via depth-resolved* FTIR and EIS.

2.3. Gloss measurements

Gloss measurements were conducted using a Byk-Gardner 6834 portable spectrometer at an incidence angle of 60°. Nine measurements were evaluated for each sample.

2.4. Fourier transform infrared (FTIR) spectroscopy imaging and focal plane array (FPA)

A Bruker Vertex 70 spectrometer equipped with a Hyperion 3000 microscope was used to perform the FTIR-ATR and FPA measurements. ATR measurements using a Specac Quest ATR accessory with a replaceable diamond internal reflection element were performed in the spectral region from 600 cm^{-1} to 4000 cm^{-1}. Background and sample measurements were collected using 250 scans at a resolution of 4 cm^{-1}. Three FTIR-ATR measurements were performed on each sample. The depth of penetration is approximately 2 μm. Focal plane array (FPA) measurements of sample cross-sections were performed as described in [26]. A schematic view of these conical holes and locations of FTIR-FPA measurements are shown in Fig. 1. Briefly, a Säberg high angle coating drill with an angle of 5.7° was used to uncover a near-horizontal cross-section of each sample. Along each cross section seven subsequent ATR-FPA measurements, each with a field of view of approximately 34 μm × 34 μm, were performed to cover a slightly larger area than the thickness of the coating. Data from the surface of the coating as well as areas further than 160 μm away from the top of the coating were excluded to ensure that the primer did not interfere with the analysis. Both backgrounds and measurements were collected at a resolution of 8 cm^{-1} using 500 scans.

Three drilled-open near-horizontal cross-sections for each sample were photographed using a AXIO Zoon V16 light optical microscope at 50× magnification to assess the coating thickness throughout the weathering process.

2.5. Electrochemical impedance spectroscopy (EIS)

The impedance measurements were performed using a Gamry REF600+ apparatus with a two-electrode configuration. The coil-coated sample (surface area of 14.6 cm^2) constituted the working electrode, and a graphite rod was used as both the counter and pseudo reference electrode. This configuration enables impedance measurements at high frequencies while minimizing artifacts that can arise from the use of a reference electrode. The measurements were conducted in a 0.5 M NaCl electrolyte at room temperature.

To assess the water uptake of the samples as a function of exposure duration to the modified QUV weathering test, a measurement protocol was optimized for very short immersion times. Thus, the diagrams were obtained every 45 s in a frequency range [10^5 Hz; 10^4 Hz] during the first 10 min of immersion and then spaced out as follows: every 5 min in the frequency range [10^5 Hz; 1 Hz] for 10 h; every 2 h in the frequency range [10^5 Hz; 10^{-2} Hz] from 10 h to 72 h of immersion; and finally, every 12 h in the frequency range [10^5 Hz; 10^{-2} Hz] from 72 h to 1 week of immersion. A 200 mV_{rms} sinusoidal voltage amplitude at a potential of

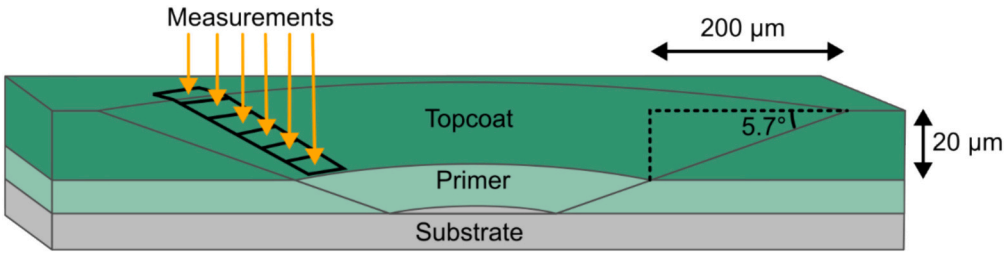

Fig. 1. Schematic view of a conical drill hole showing the locations of subsequent FTIR-ATR FPA measurements. Not to scale.

0 V *vs* OCP (open circuit potential), with 8 points/decade, was applied for all the measurements. For the EIS study of capacitive coatings in the absence of corrosion processes, increasing the applied voltage is not an issue as long as the impedance response remains linear with respect to the applied field (such linearity was checked up to 1000 mV_{rms}).

3. Results and discussion

3.1. Gloss loss

Fig. 2 shows the gloss variation for the reference and polyester/melamine samples subjected to the modified QUV test. After 250 h, no gloss variation was observed compared with the reference sample. However, from 500 h to 2000 h of exposure, a progressive decrease in gloss was noted, ranging from approximately −35 % to −85 %, with a nearly constant variation between 1500 h and 2000 h. Gloss is related to the surface morphology, which is dependent on factors such as matting agents, pigmentation, localized damages across the coating surface and photodegradation reactions [22]. The latter causes modifications in the chemical structure, which can result in an increase in surface roughness and a loss of gloss [20].

3.2. Chemical structure of the coil-coating as a function of the QUV exposure time

Fig. 3a shows the FTIR-ATR spectra of the reference sample and of the samples subjected to the modified QUV test. The most notable bands are indicated by arrows, and the intensity was normalized against the band at 1375 cm^{-1}, which is associated with –CH group chain deformation (Fig. 3c). Bands associated with $–CH_2$ and $–CH_3$ groups stretching vibrations are located at approximately 2800 cm^{-1} to 3000 cm^{-1} and are surrounded by multiple wide bands associated with –OH and –NH groups stretching vibrations from 2300 cm^{-1} to 3700 cm^{-1} (Fig. 3b). The large band centered at approximately 1720 cm^{-1} is assigned to the stretching mode of the carbonyl group (—C═O). Aromatic groups in the polymer backbone show bands with low intensities at 1608 cm^{-1} and 1580 cm^{-1}, whereas broader bands at approximately 1600 cm^{-1} to 1650 cm^{-1} can be attributed to the amide I group (—C═O stretching mode) and the amine group (–NH bending mode). The band at 1550 cm^{-1} has multiple components and has previously been assigned to a combination of quadrant stretching of the melamine-triazine group, as well as side chain –CN contraction and –CH group bending vibrations (Fig. 3c).

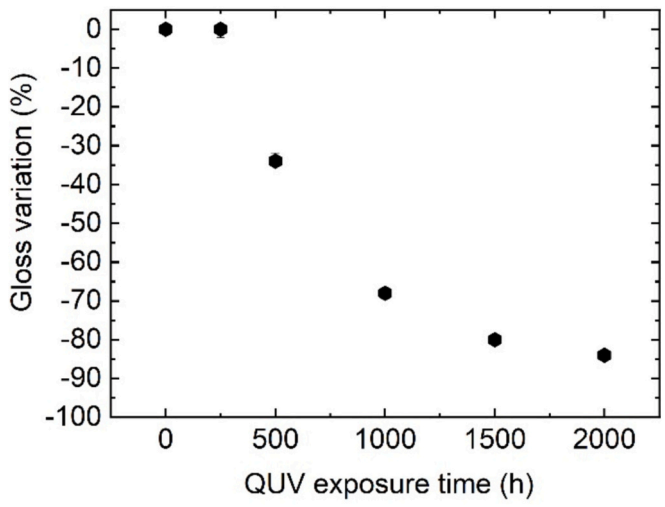

Fig. 2. Gloss variation of the polyester/melamine system as a function of the modified QUV test exposure time.

With increased exposure time to the modified QUV artificial weathering test, multiple changes can be observed across the spectral range. First, an increase in the intensity of the bands from 2300 cm^{-1} to 3700 cm^{-1} with increasing QUV exposure time is noted and is related to the photooxidation of the polymer matrix. The appearance of a shoulder at approximately 1780 cm^{-1} is subsequently observed with increasing QUV exposure time, which is attributed to the formation of multiple degradation products, including anhydrides, peracids, peresters, and lactones [23,28,35,36]. Finally, a decrease in intensity and broadening of the band at 1550 cm^{-1} with increasing QUV exposure time can be observed. This is related to changes in the environment surrounding the central triazine group in the melamine crosslinker. A schematic of the crosslinked melamine is shown in Fig. 3c. Although multiple reactions occur simultaneously, some consider the breaking of certain ether linkages between melamine and polyester to be the most significant factor. However, other reactions such as abstraction of hydrogen atoms from the CH_2 groups between the ether and the triazine ring, enabling further reactions could also have an effect [37,38].

Three parameters, as presented in Fig. 4, were considered to quantify the changes observed in the infrared spectra as a function of the exposure time to the weathering test: the oxidative index (OI) (Fig. 4b), the intensity of the 1780 cm^{-1} band, referred to as the peracid band (Fig. 4c), and the melamine substitution functionality loss (MSFL) (Fig. 4a). The OI index (Fig. 4b), which is correlated with the photooxidation of the coating [22,32,39,40], describes the area growth underneath the –OH band from 2400 cm^{-1} to 3700 cm^{-1} and is normalized against the –CH bands at approximately 2700 cm^{-1} to 3000 cm^{-1}. The peracid band (Fig. 4c), related to the formation of degradation products, is reported as the absorbance of this band calculated using an extrapolated linear baseline anchored between two points, 2000 cm^{-1} and 1830 cm^{-1}. Finally, the MSFL (Fig. 4a), related to the degradation reactions in polyester/melamine systems [22,23,26], is the percentage decrease in the band intensity at 1550 cm^{-1} normalized against the band assigned to the –CH band at approximately 1375 cm^{-1}. Notably, since MSFL measures the decrease in band intensity, the theoretical maximum value that can be reached is 100 %, whereas OI measures the increase in –OH groups (and, to some degree, –NH groups) hence, its values regularly exceed 100 % [22,32,41].

For the sample subjected to the modified QUV test for 250 h, the three indexes are comparable to those of the reference sample, suggesting that no major degradation reaction due to UV radiation initially occurs. However, after 250 h of exposure, both the OI and MSFL indexes progressively increases, along with the formation of degradation

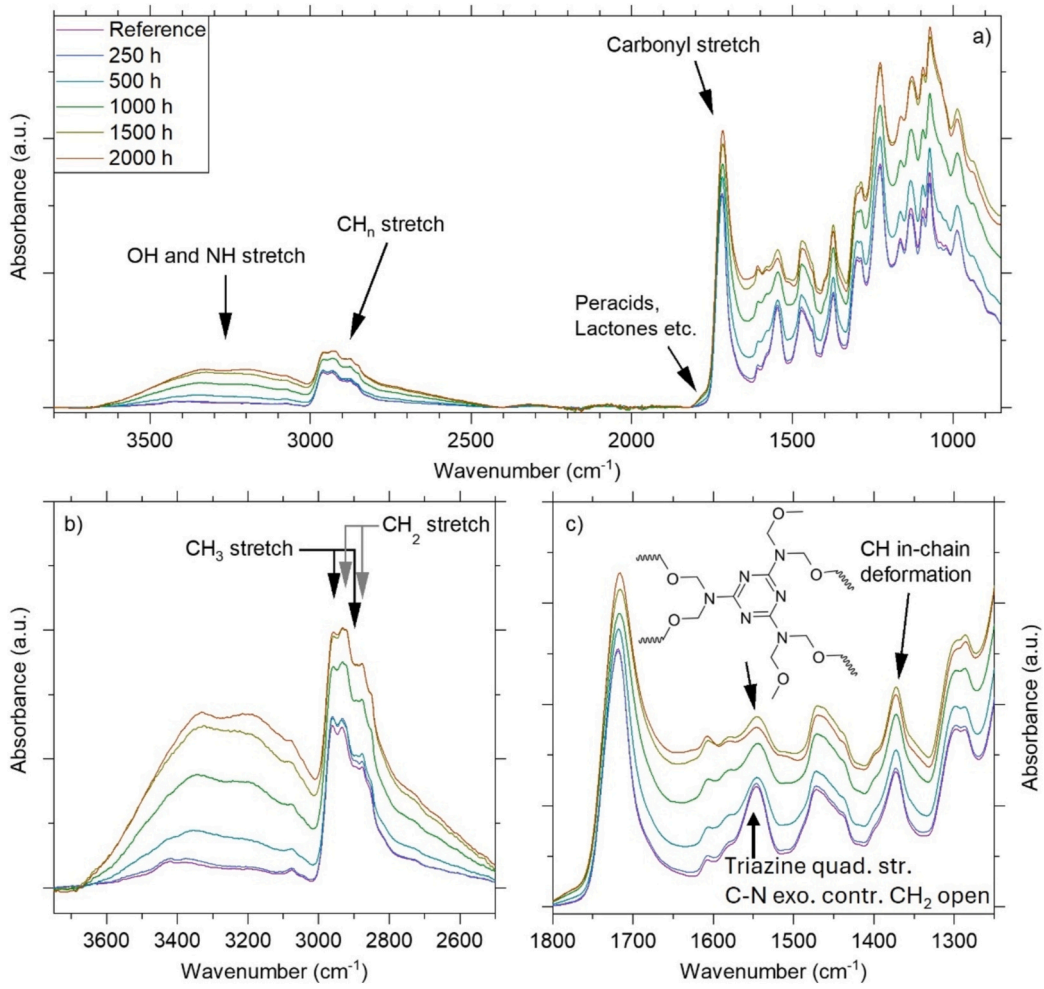

Fig. 3. FTIR-ATR spectra of the reference coil-coating and of the samples exposed from 250 h to 2000 h to the modified QUV test.

products, as indicated by the peracid band. Except for the OI index, the MSFL and peracid band absorbance values appeared relatively stable between 1500 h and 2000 h of exposure. The variation in the considered indexes is in agreement with the gloss variation (Fig. 2), indicating that gloss loss is correlated with the chemical changes occurring at the coating surface.

Finally, FTIR-ATR FPA measurements were conducted across the near-horizontal drilled open cross-sections for the reference and for the QUV-exposed samples. As previously reported the melamine band intensity (1550 cm^{-1}) varies across the bulk of the coating, tending to be lower close to the surface [27,42,43]. Because of this, the reference value used to calculate the MSFL was determined *via* linear interpolation of the normalized 1550 cm^{-1} band intensity across the cross-section of the reference sample. Heatmaps of the near-horizontal cross sections of the studied samples are presented in Fig. 5. The heatmaps show areas measuring approximately 160 μm × 32 μm in the near-horizontal cross-sections, corresponding to the outermost 16 μm of the coating. The region at the top of the maps represents degradation closest to the surface, whereas the values further down represent degradation into the bulk. The reference shows small variations in the MSFL, on the scale of ±10 %. This is consistent with local points with higher melamine crosslinker contents, which are known to be present on the micrometric scale [5–8]. Small variations in band intensity could also be caused by changes in signal-to-noise ratio, caused by, for example, limited sample-IR contact. Similar to the FTIR-ATR data collected from the surface, no major chemical degradation occurred during the first 250 h of exposure. After this, chemical changes began to occur, with greater degradation observed closer to the coating surface and less degradation observed further into the bulk. To better visualize the changes occurring throughout the cross-section, the average MSFL across 1.8 μm sections, as well as the standard deviation within each section, are presented in Fig. 6. The chemical degradation of the coating increased with increasing exposure time to the QUV test on both the surface and the bulk of the sample, as indicated by the increase in the MSFL value, except for the sample exposed for 250 h. For the samples exposed from 500 h to 2000 h, the chemical degradation was greater at the surface and gradually decreased to approximately 4 μm, remaining stable throughout the rest of the analyzed cross-section (16 μm). This is presumably due mainly to the limited oxygen diffusion and the limited penetration depth of UV radiation [9–11].

To summarize, the QUV accelerated weathering test induced chemical degradation of the coil-coating from 500 h to 2000 h of exposure, leading to changes in the chemical structure, including changes in the melamine groups and formation of polar groups such as hydroxyl, peracid, amide and amine groups. Degradation was more pronounced closer to the coating surface, extending down to 4 μm into the bulk, which resulted in gloss loss in the samples. However, from 4 μm to 16 μm into the bulk of the coating, chemical degradation remained stable. In the next section, the influence of this chemical degradation on the water uptake and plasticization of the coating, investigated by EIS measurements, is discussed.

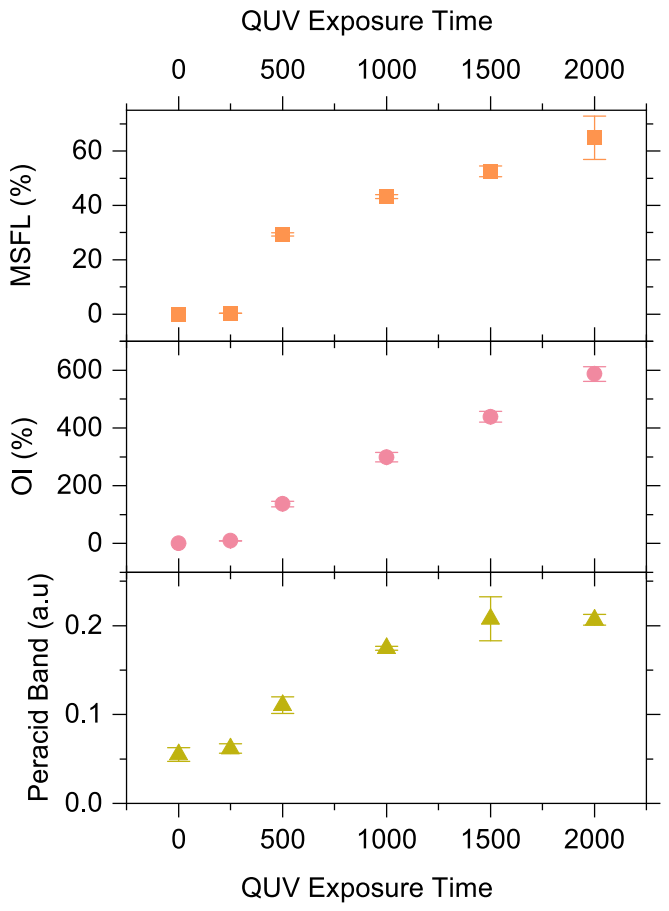

Fig. 4. Crosslinker degradation index (MSFL), oxidative index (OI), and intensity of the 1780 cm^{-1} shoulder (peracid band) of the coil-coated samples as a function of the modified QUV test exposure time considering the standard deviation from three independent measurements.

3.3. EIS spectra as a function of the QUV exposure time and immersion time in the electrolyte

The reference polyester/melamine coil-coated steel and the samples exposed for 250 h, 500 h, 1000 h, 1500 h, and 2000 h to the modified QUV test were characterized by EIS during 1 week of immersion (168 h) in a 0.5 M NaCl electrolyte at room temperature. As an example, Fig. 7a and b present the EIS spectra in Bode coordinates for the studied samples after 2 h and 24 h of immersion, respectively. The impedance modulus is characterized by a quasi-linear increase with decreasing frequency, indicating the capacitive behavior of the studied systems. For both immersion times, the impedance moduli are superimposed at high frequencies and slightly decrease at low frequencies as the QUV exposure time increases. Moreover, the impedance modulus values remain higher than 10^{10} Ω cm^2 at low frequency, without the appearance of blistering and/or corrosion. The phase angle values also remain high, between −88° and −75°, which is consistent with the capacitive behavior of the systems. This EIS response attests to the protective properties of the coating [33,34,44,45]. The phase angle diagrams change as the QUV exposure time and immersion time in the NaCl solution increase. For the reference coil-coating, a second time constant ([10^{-2} Hz; 10^{-1} Hz]) is

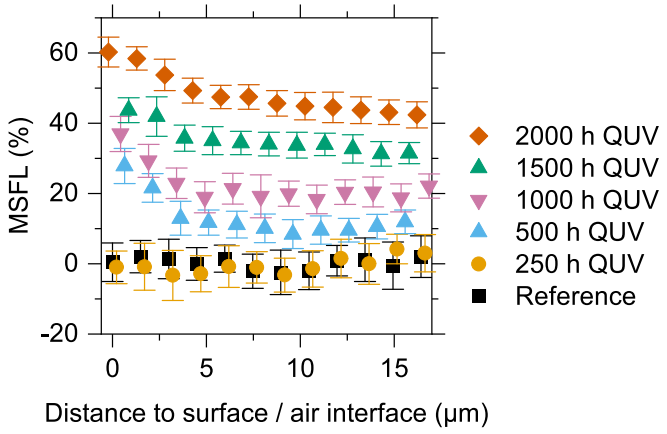

Fig. 6. MSFL index as a function of depth in coating cross-sections of the reference and of the samples exposed from 250 h to 2000 h to the modified QUV test.

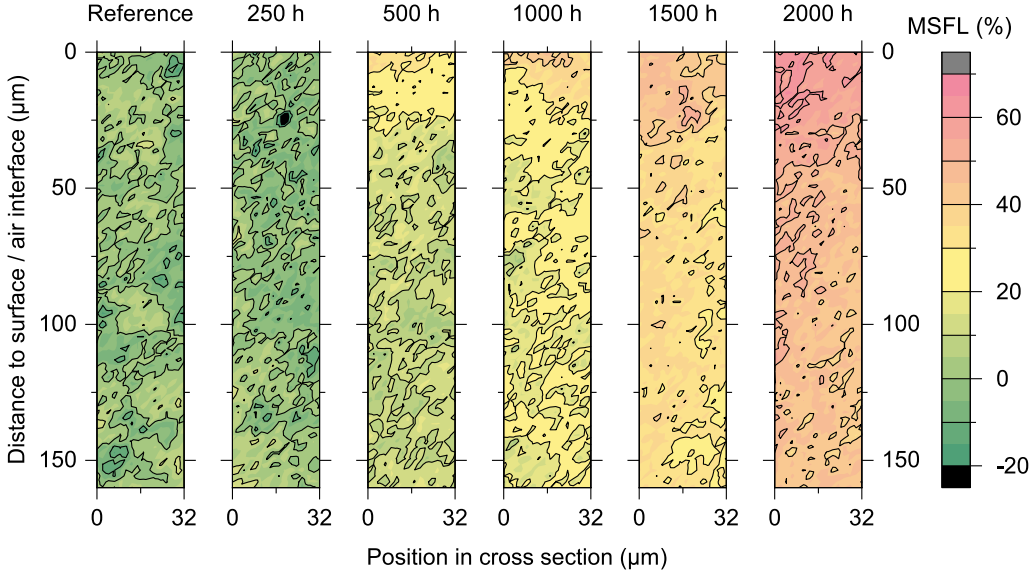

Fig. 5. Spatially resolved crosslinker degradation index (MSFL) of the coating cross-section of the reference sample and the samples exposed from 250 h to 2000 h to the modified QUV test.

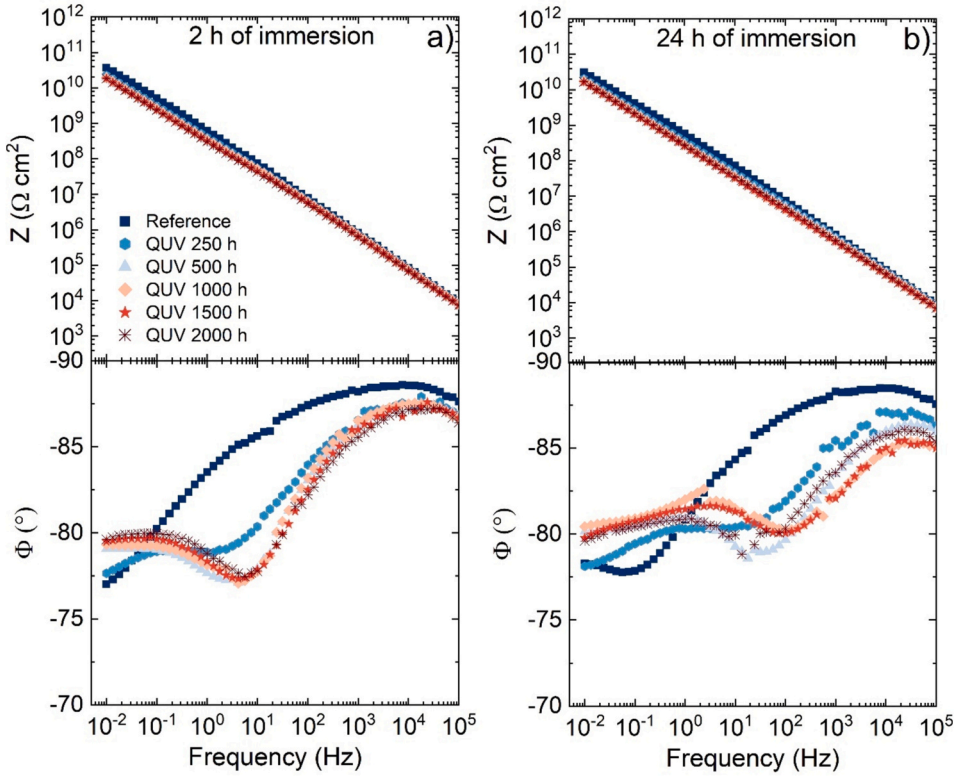

Fig. 7. EIS measurements (Bode plots) obtained for the reference coil-coating and the samples exposed from 250 h to 2000 h to the modified QUV test after a) 2 h and b) 24 h of immersion in the 0.5 M NaCl solution at room temperature.

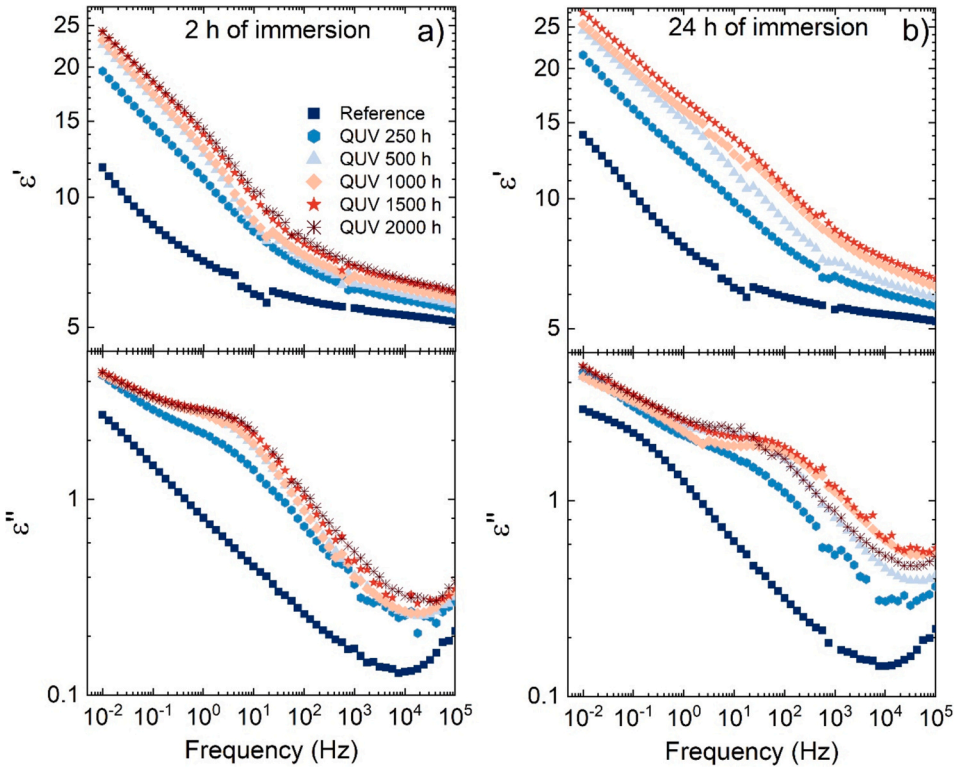

Fig. 8. Complex permittivity spectra obtained for the reference coil-coating and the samples exposed from 250 h to 2000 h to the modified QUV test after a) 2 h and b) 24 h of immersion in the 0.5 M NaCl solution.

observed after 24 h of immersion. For the QUV-exposed coil-coatings, the time constant ([10^{-2} Hz; 1 Hz]) is observed from 2 h of immersion and shifts toward higher frequencies with increased QUV exposure times and immersion times in the NaCl solution. It has been previously shown that this time constant can be attributed to the dielectric manifestation of the polymer matrix glass transition (α-mode) [33,34,44].

To emphasize the dipolar phenomena, the impedance spectra were transformed to complex dielectric permittivity, according to Eq. 1.

$$\varepsilon^*(\omega) = \varepsilon'(\omega) - i\,\varepsilon''(\omega) = \frac{-Z''(\omega)}{\omega C_V\left[(Z'(\omega))^2 + (Z''(\omega))^2\right]} - i\frac{Z'(\omega)}{\omega C_V\left[(Z'(\omega))^2 + (Z''(\omega))^2\right]} \quad (1)$$

with $C_v = \frac{\varepsilon_v A}{l}$ where ω is the angular frequency, $Z'(\omega)$ and $Z''(\omega)$ are the real and imaginary parts of the impedance modulus, $\varepsilon'(\omega)$ and $\varepsilon''(\omega)$ are the real and imaginary parts of the complex permittivity and C_v the capacitance of the equivalent vacuum-filled (ε_v of a value of 8.85 × 10^{-12} F m^{-1} is the vacuum permittivity) parallel plate capacitor formed by two electrodes of area A and separated by the distance l. A represents the area of the EIS cell (14.6 cm^2), and l represents the coating thickness (25 μm). From the optical microscopy of the drill holes, it was verified that the coating thickness remained relatively constant throughout the weathering process. The average coating thickness varied by approximately 1 μm throughout the exposure to the modified QUV test. No clear trend toward a decrease in coating thickness was noted.

Fig. 8 shows the real $\varepsilon'(\omega)$ and imaginary $\varepsilon''(\omega)$ parts of the permittivity spectra for the reference coil-coating and the systems exposed to the QUV modified test for 2 h (Fig. 8a) and 24 h (Fig. 8b) of immersion. The real part, $\varepsilon'(\omega)$, is associated with the energy storage of the sample and exhibited a step-like decrease in permittivity with increasing frequency for all the studied conditions [46]. An increase in the real permittivity values is observed for all the recorded frequencies with increasing QUV exposure time from 250 h to 2000 h, whether for 2 h or 24 h of immersion in the NaCl solution. Furthermore, the permittivity values for 24 h of immersion are greater for all the studied systems than those observed for 2 h of immersion. The $\varepsilon'(\omega)$ values at high frequency are used to calculate the water uptake of the samples as a function of both the immersion time in the NaCl solution and the QUV exposure time. The water uptake of the samples is discussed in Section 3.3.1.

The imaginary part, $\varepsilon''(\omega)$, is related to the energy dissipation of the sample, resulting from electrical charge carrier transport or molecular mobility modes [46,47]. The peak in $\varepsilon''(\omega)$, which corresponds to a relaxation time (τ), describes the second time constant observed in the phase angle spectra (Fig. 7) [46]. The time constant is visible after 24 h of immersion for the reference coating and after only 2 h of immersion for the QUV exposed samples. As observed from the Bode plots (Fig. 7), this time constant shifts to higher frequencies with increasing QUV exposure time and immersion time in the electrolyte solution and it is analyzed in Section 3.3.2.

3.3.1. Water uptake analysis

To assess the water uptake of the samples, first the real permittivity values were extracted at 10^4 Hz and 10^5 Hz as a function of the immersion time (ε'_t). Although the variations in ε'_t were generally similar across the chosen frequencies (data not shown), the frequency of 10^5 Hz was selected to calculate the water uptake (Fig. 9a). For frequencies lower than 10^4 Hz, the time constant associated with the dielectric manifestation of the glass transition could influence the water uptake values. The increase in the ε'_t values over immersion time for all tested samples indicated water absorption. Due to the significant difference in permittivity between a polymer in the dry state ($\varepsilon_{polymer} \sim 3$–$8$) and water ($\varepsilon_{water} = 80$), the permittivity value of the system increases with increasing water uptake. Their variations will be discussed in the context of the water uptake values.

Second, $\varepsilon'_{t=0}$, corresponding to the polymer permittivity in the dry state, was determined by extrapolation of the permittivity for short immersion times from the ε'_t graph (Fig. 9a) and is presented in Fig. 9b. An increase in $\varepsilon'_{t=0}$ is noted, from 4.7 to 5.3, with increasing QUV exposure time up to 2000 h. The increase in $\varepsilon'_{t=0}$ values suggests a modification of the polyester/melamine system in the dry state (before immersion) due to UV radiation and condensation cycles. The chemical changes observed from the FTIR analyses, such as the loss of cross-linker/polyester bonds and the formation of polar groups due to photooxidation (Section 3.2), could increase the polymer's mobility, resulting in higher $\varepsilon'_{t=0}$ values [48]. It is important to note that the permittivity values of each sample cannot be measured by EIS before QUV exposure. This would require immersion of the sample in the NaCl solution, which can modify the ageing processes. In previous works, a permittivity variation of ±0.15 in the reference sample was observed, depending on the measurement location on the same coil-coated panel, due to local variations in composition and/or morphology (data not shown). This may explain the higher permittivity value measured after 250 h of ageing, indicating that further analysis of the impedance data is necessary.

Next, water uptake was calculated with a linear rule of mixtures [33,34,49–51], according to Eq. 2, which considers the coating and the absorbed water.

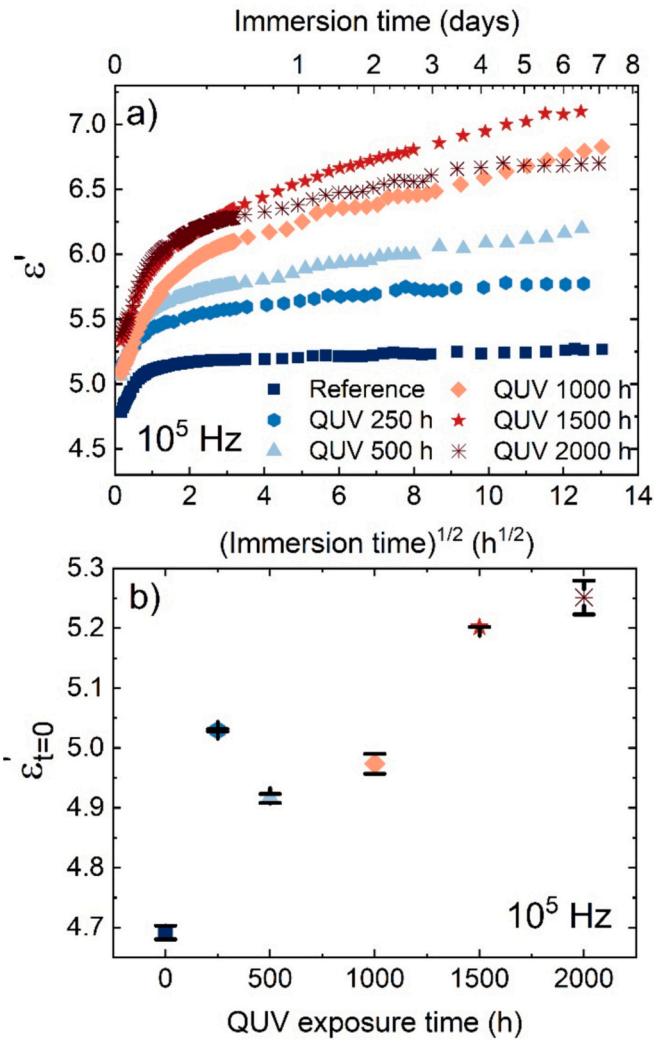

Fig. 9. a) Variation in the real part of the permittivity ε'_t *vs* immersion time for the studied samples. b) Values of $\varepsilon'_{t=0}$ extrapolated from the first immersion times in figure a) for the coil-coated steel samples exposed to the modified QUV test.

$$\Phi_t\ (\text{vol\%}) = \frac{\varepsilon'_t - \varepsilon'_{t=0}}{\varepsilon'_{H_2O} - \varepsilon'_{t=0}} \quad (2)$$

where, Φ_t is the water uptake as a function of the immersion time (vol %), ε'_t is the real part of the coating permittivity at a chosen frequency (here, 10^5 Hz) over immersion time, $\varepsilon'_{t=0}$ is the coating permittivity in the dry state (before immersion) and ε'_{H_2O} is the water permittivity at 20 °C (80) [52].

The water uptake values as a function of the square root of the immersion time are reported in Fig. 10. The diffusion behavior does not follow a classic Fick's law, as is commonly observed for many polymers, particularly when they are in a rubbery state, and the penetrant has less mobility than the chain segments do [18,53]. Two regions are observed for all the studied conditions, a first linear increase in water uptake values corresponding to a relatively quick water absorption (region I), indicative of Fickian behavior, and a subsequent much slower linear increase (region II), corresponding to non-Fickian behavior. A Fickian mechanism is associated with little or no interaction between the water and the polymer: diffusion would take place in random jumps, probably between vacant sites in the coating, such as porosities and/or low crosslinked density areas [45]. Region II would correspond to a slower diffusion of water at the molecular scale, in interaction with the polymer chains [34]. The total water uptake values and the corresponding immersion times in regions I and II differ for each sample. For the reference sample and the one exposed to the QUV test for 250 h, the water uptake reached approximately 0.55 vol% during the first hour of immersion (region I). In region II, the water uptake values were approximately 0.73 vol% and 0.94 vol%, respectively. The small differences in the water uptake values for these two samples are in agreement with the limited variation in the extracted infrared indexes (Fig. 5). For the 500 h exposed sample, water uptake values in region I (within the first hour) and region II were 0.93 vol% and 1.7 vol%, respectively. For the samples exposed for 1000 h and 1500 h, the water uptake in region I was approximately 1.4 vol% within the first 6 h of immersion, and in region II, it was 2.4 vol% and 2.5 vol%, respectively. Finally, for the 2000 h exposed sample, water uptake in regions I and II was approximately 1.4 vol% and 1.9 vol%, respectively. Overall, an increase in water uptake values in regions I and II was observed with increasing QUV exposure time, except for the 2000 h exposed sample, where water uptake values in region II were lower than in the 1000 h and 1500 h exposed samples. None of the studied samples reached a steady-state within the duration of the experiment.

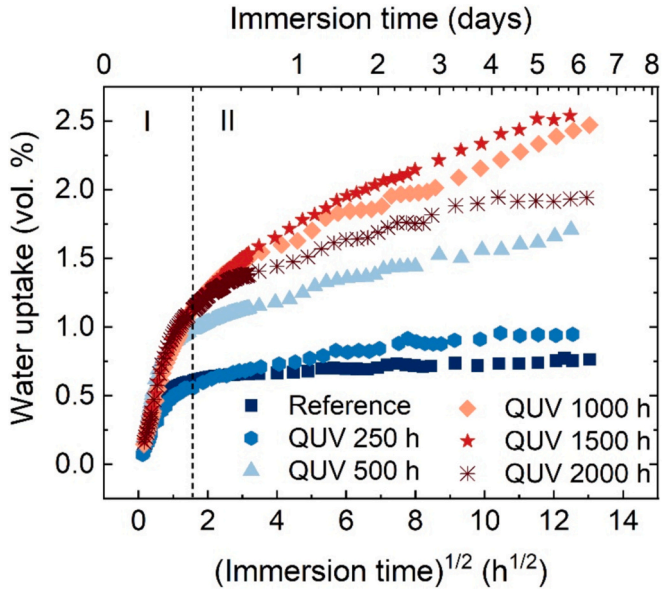

Fig. 10. Water uptake as a function of immersion time in the 0.5 M NaCl solution for the reference coil-coating and the coatings exposed to the modified QUV test for 250 h, 500 h, 1000 h, 1500 h and 2000 h. The dotted line is only illustrative of the separation of the two regions.

Finally, the water diffusion coefficients (D_w) were calculated for all the studied conditions according to Eq. 3 [53,54].

$$D_w = \left(\frac{P_I \times l}{\Phi_\infty} \times \frac{1}{4}\right)^2 \pi \quad (3)$$

where P_I corresponds to the slope of the curve for a short immersion time (region I) (Fig. 10), l is the thickness of the coating (25 µm) and Φ_∞ is the water uptake value at saturation (Fig. 10).

To assess the water uptake value at saturation (Φ_∞), the Fickian part was dissociated from the total water uptake by subtracting the linear increase observed in region II, as described in our previous work [33]. The slope values in region II were considered for three immersion time intervals: from 4 h to 196 h, from 16 h to 196 h, and from 4 h to 100 h. The slope values of region I (P_I) and II (P_{II}) for the time interval from 16 h to 196 h, the water uptake value at saturation (Φ_∞) and the water diffusion coefficient (D_w) for each sample are given in Table 1.

The slope value of region I for the sample exposed for 250 h was comparable to that of the reference sample. For the other exposed samples, the P_I were relatively similar. The value of the slope seemed to increase with increasing QUV exposure time, which indicated an acceleration of short-time water uptake. At the same time, the values at saturation (Φ_∞) increased with increasing QUV exposure time, with values remaining somewhat constant from 1000 h to 2000 h of exposure. The calculated D_w values varied between 0.15×10^{-12} m^2 s^{-1} and 0.09×10^{-12} m^2 s^{-1}, comparable to the values previously reported for other polyester coil-coatings [33,48]. Two behaviors can be distinguished from the D_w values. For the reference sample and the ones exposed for 250 h and 500 h to the modified QUV test, the D_w values varied between 0.12×10^{-12} m^2 s^{-1} and 0.18×10^{-12} m^2 s^{-1}. For the three remaining samples, the D_w values varied between 0.06×10^{-12} m^2 s^{-1} and 0.09×10^{-12} m^2 s^{-1}. Schachinger *et al.* [48] reported the same decrease in the water diffusion coefficient for polyester coatings with increasing UV exposure time, which was suggested to be related to the photooxidation of the upper layer of the coating resulting in a decrease in the diffusion coefficient. Infrared analyses showed that the polymer matrix was affected by the accelerated QUV test, indicating changes in the polyester/crosslinker bonds and the formation of polar groups such as hydroxyls, lactones, and peroxides. In addition, the possible leaching of pigments could create additional free sites, increasing water absorption. However, infrared analyses do not allow to conclude on the creation of additional porosities or pathways accessible to water, which could explain the faster penetration (P_I) and greater quantity (Φ_∞).

Regarding the slope values of region II, they progressively increased from the 250 h to the 1000 h exposed samples compared to the reference. The slope value of the sample exposed for 1500 h was similar to that of the sample exposed for 1000 h. Conversely, for the sample exposed for 2000 h, the P_{II} is similar to that of the sample exposed for 500 h. It is worth noting that this slope is sometimes attributed to the "swelling" of the polymer [48,55]. However, this concept is rather imprecise and, depending on the author, it may refer to macroscopic geometric swelling (increase in thickness) or an increase in free volume on a macromolecular scale (enhanced water/polymer interaction) [20,55]. The following section provides a more detailed analysis of this second region by analysing the time constant associated with the glass transition of the polymer.

3.3.2. Time constant analysis

The time constant in the $\varepsilon''(\omega)$ spectra (Fig. 8) was not distinguishable enough to extract a relaxation time, usually adjusted with the Havriliak-Negami equation [56]. Therefore, the dielectric loss factor, tan(δ), was calculated according to Eq. 4 to exacerbate the time constant [46] and to follow its variation during immersion.

Table 1
Slope values in region I during the first hour of immersion (P_I) and II (P_{II}) considered for immersion times from 16 h to 196 h, the water uptake value at saturation (Φ_∞) and the water diffusion coefficient (D_w). The standard deviation of D_w values was calculated from the considered time intervals.

	Reference	250 h	500 h	1000 h	1500 h	2000 h
P_I ($h^{-1/2}$)	0.78	0.70	1.29	0.93	1.04	1.13
Φ_∞ (vol%)	0.63	0.64	0.93	1.17	1.14	1.17
D_w (10^{-12} m^2 s^{-1})	0.15 ± 0.01	0.12 ± 0.02	0.18 ± 0.01	0.06 ± 0.01	0.08 ± 0.02	0.09 ± 0.01
P_{II} (10^{-4} $h^{-1/2}$)	1.0	2.5	5.6	9.5	10	5.7

$$tan(\delta) = \frac{\varepsilon''(\omega)}{\varepsilon'(\omega)} \quad (4)$$

As an example, the tan(δ) of the reference sample is shown in Fig. 11 for three immersion times. The time constant shifts toward higher frequencies with increasing immersion time.

The relaxation times (τ), corresponding to the maximum of the peak (dotted line in Fig. 11), were extracted for the studied samples and are shown in Fig. 12. A decrease in the relaxation time values is observed with increasing immersion time in the 0.5 NaCl solution, regardless of the QUV exposure time. The simultaneous decrease in the τ values and increase in the water uptake values suggest plasticization of the polymer matrix [34]. The presence of water increases the free volume by perturbing the physical bonding of the inter- and intra-polymer chains and thus facilitating the molecular chain mobility involved in the α-mode. The latter manifests at higher frequencies and, therefore, smaller relaxation times. The relaxation times for the shortest immersion times were similar, regardless of the QUV exposure time, but lower than those for the reference sample (without ageing). The wet cycles at 40 °C during the accelerated ageing test can induce a strong change in the molecular mobility of the polymer, similar to what was demonstrated in a previous work for successive immersion and drying cycles [34]. This suggests that while UV-induced degradation affects the chemical structure and both the bulk and surface properties of the coating, the dominant mechanism influencing molecular mobility appears to be water absorption during the modified QUV weathering test.

For immersion times greater than 24 h, a noticeable and progressive decrease in the relaxation time values is observed. The greater the QUV exposure time (from 250 h to 1500 h), the faster the decrease. Interestingly, the relaxation time values are similar for the samples exposed for 1000 h and 1500 h, whereas for the sample exposed for 2000 h, they increase and are nearly identical to those of the sample exposed for 500 h. This pattern suggests that the polymer chain scission, the formation of

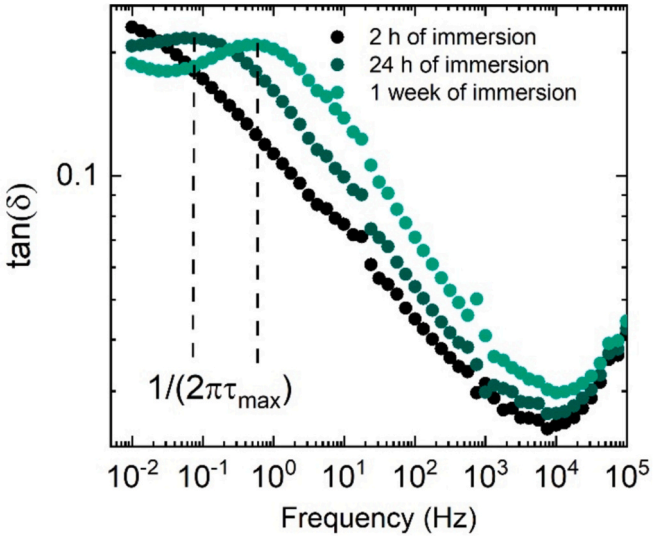

Fig. 11. tan(δ) calculated from the EIS diagrams for the reference coil-coated steel after 2 h, 24 h and 1 week of immersion in the 0.5 M NaCl solution.

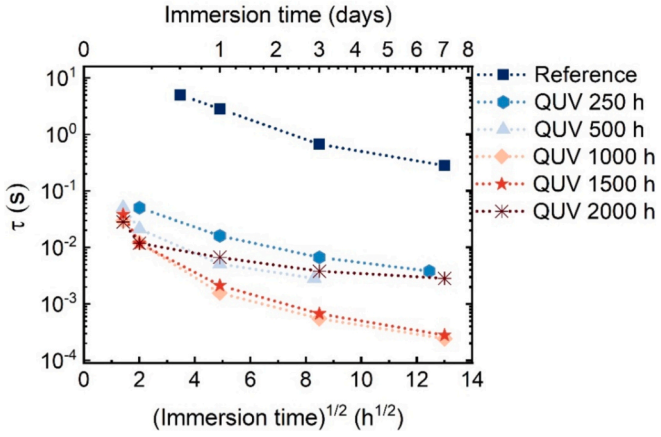

Fig. 12. Time constant (τ) *vs* immersion time in the 0.5 M NaCl solution for the reference coil-coated steel and the samples exposed to the modified QUV test.

hydroxyl groups, and the smaller degradation products such as peracids may increase chain mobility in the polymer matrix. This is consistent with the observed increase in the $\varepsilon'_{t=0}$ values and the decrease in τ for the initial immersion times. The increase in the τ values for the sample exposed for 2000 h indicates that the degradation reactions after long times of QUV exposure are different from those in the early stages. One possibility is that new degradation products or crosslinking reactions, which are not easily identified from the FTIR-spectra, could be formed for severe levels of degradation. This could lead to a decrease in the free volume within the polymer matrix, an increase in relaxation times (Fig. 12) and a decrease in water uptake values (Fig. 10). Another possibility could be that the difference between the degradation in the bulk and the surface of the coating, as quantified using the MSFL index, decreases with increasing exposure time and leads to a more homogeneous material. The variations in relaxation times with increasing QUV exposure time are in correlation with the variations in the slope values in region II (Table 1) and the total water uptake at the end of the EIS measurement (1 week of immersion) (Fig. 10). The non-Fickian nature of the water uptake of this system seems to be linked to the effect of water on the mobility of the polymer chains (plasticization phenomena) [57].

4. Conclusions

In this study, *ex situ* FTIR-ATR chemical imaging and *in situ* EIS were combined to investigate the ageing process of polyester/melamine coil-coated steel. Infrared measurements indicated that chemical degradation of the polymer matrix began between 500 h and 2000 h of QUV exposure. This degradation resulted in chain scission from the breakage of polyester/melamine bonds, the formation of polar groups such as hydroxyl group, and the degradation products such as peracid and amine groups. Degradation was more pronounced near the coating surface, extending down to 4 μm, but significant degradation was observed through the whole topcoat, particularly after prolonged exposure. UV degradation and condensation cycles increased chain mobility in the polymer matrix, as revealed by *in situ* EIS measurements,

which showed significantly increased water uptake with increasing QUV exposure time. The water sorption curves revealed two regions: an initial rapid increase attributed to Fickian behavior and a slower linear increase describing non-Fickian behavior. The first region, associated with the diffusion of water into vacant sites within the coating, such as porosities, accelerated with increasing QUV exposure time. The second region was influenced by water/polymer interactions. The analysis of the time constant (τ), which is related to the dielectric manifestation of the glass transition, indicated the plasticization of the polymer matrix with water uptake, which was partly responsible for the non-Fickian behavior observed in the second region. Despite the UV degradation, the coating's protective properties remained effective, as evidenced by the consistently high impedance modulus at low frequency, which was unaffected by increasing the UV exposure time or immersion duration in the NaCl solution. This methodology allows the identification of ageing markers and holds promise for studying other systems to establish links between UV degradation mechanisms, water uptake, and the molecular mobility of polymer anticorrosion coatings.

CRediT authorship contribution statement

Deni Jero: Writing – original draft, Methodology, Investigation, Formal analysis, Data curation, Conceptualization. **Alexander Wärnheim:** Writing – original draft, Methodology, Investigation, Formal analysis, Data curation, Conceptualization. **Nicolas Caussé:** Writing – review & editing, Validation, Supervision, Resources, Project administration, Methodology, Investigation, Formal analysis, Data curation, Conceptualization. **Nathalie LeBozec:** Writing – review & editing, Validation, Supervision, Resources, Project administration, Methodology, Funding acquisition, Formal analysis, Data curation, Conceptualization. **Nadine Pébère:** Writing – review & editing, Validation, Supervision, Resources, Project administration, Methodology, Formal analysis, Data curation, Conceptualization. **Dan Persson:** Writing – review & editing, Validation, Supervision, Methodology, Investigation, Formal analysis, Data curation, Conceptualization. **Dominique Thierry:** Writing – review & editing, Validation, Supervision, Resources, Project administration, Methodology, Funding acquisition, Formal analysis, Conceptualization.

Declaration of competing interest

The authors declare that they have no known competing financial interests or personal relationships that could have appeared to influence the work reported in this paper.

Acknowledgments

This work has been partially funded by the Swedish Foundation for Strategic Research (SSF) grant number FID18-0034 and the Member Research Consortium on Coil Coated Materials. The authors gratefully acknowledge Mélissa Bonnet and Laura Manika for their help in conducting the EIS measurements.

Data availability

Data will be made available on request.

References

[1] T. Prosek, D. Thierry, A model for the release of chromate from organic coatings, Prog. Org. Coat. 49 (2004) 209–217, https://doi.org/10.1016/j.porgcoat.2003.09.012.
[2] A.C. Bastos, A.M.P. Simões, Effect of deep drawing on the performance of coil-coatings assessed by electrochemical techniques, Prog. Org. Coat. 65 (2009) 295–303, https://doi.org/10.1016/j.porgcoat.2009.01.002.
[3] W. Funke, Blistering of paint films and filiform corrosion, Prog. Org. Coat. 9 (1981) 29–46, https://doi.org/10.1016/0033-0655(81)80014-3.
[4] O. Negele, W. Funke, Internal stress and wet adhesion of organic coatings, Prog. Org. Coat. 28 (1996) 285–289, https://doi.org/10.1016/0300-9440(95)00606-0.
[5] F. Zou, D. Thierry, Localized electrochemical impedance spectroscopy for studying the degradation of organic coatings, Electrochim. Acta 42 (1997) 3293–3301, https://doi.org/10.1016/S0013-4686(97)00180-1.
[6] D.R. Bauer, Degradation of organic coatings. I. Hydrolysis of melamine formaldehyde/acrylic copolymer films, J. Appl. Polym. Sci. 27 (1982) 3651–3662, https://doi.org/10.1002/app.1982.070271002.
[7] B.W. Johnson, R. McIntyre, Analysis of test methods for UV durability predictions of polymer coatings, Prog. Org. Coat. 27 (1996) 95–106, https://doi.org/10.1016/0300-9440(94)00525-7.
[8] H.K. Hardcastle, W.L. Meeks, Considerations for characterizing moisture effects in coatings weathering studies, J. Coat. Technol. Res. 5 (2008) 181–192, https://doi.org/10.1007/s11998-007-9078-0.
[9] W.R. Zhang, C. Lowe, R. Smith, Depth profiling of coil coating using step-scan photoacoustic FTIR, Prog. Org. Coat. 65 (2009) 469–476, https://doi.org/10.1016/j.porgcoat.2009.04.005.
[10] J.F. Rabek, Polymer Photodegradation, Springer Netherlands, 1995, https://doi.org/10.1007/978-94-011-1274-1.
[11] S. Shreepathi, S.M. Naik, M.R. Vattipalli, Water transportation through organic coatings: correlation between electrochemical impedance measurements, gravimetry, and water vapor permeability, J. Coat. Technol. Res. 9 (2012) 411–422, https://doi.org/10.1007/s11998-011-9376-4.
[12] C. Vosgien Lacombre, G. Bouvet, D. Trinh, S. Mallarino, S. Touzain, Effect of pigment and temperature onto swelling and water uptake during organic coating ageing, Prog. Org. Coat. 124 (2018) 249–255, https://doi.org/10.1016/j.porgcoat.2017.11.022.
[13] N.A. Brunt, Blistering of paint layers as an effect of swelling by water, J. Oil Color Chem. Assoc. 47 (1964) 31–42.
[14] L. Fedrizzi, F. Deflorian, G. Boni, P.L. Bonora, E. Pasini, EIS study of environmentally friendly coil coating performances, Prog. Org. Coat. 29 (1996) 89–96, https://doi.org/10.1016/S0300-9440(96)00620-0.
[15] F. Mansfeld, M.W. Kendig, S. Tsai, Evaluation of corrosion behavior of coated metals with AC impedance measurements, Corrosion 38 (1982) 478–485, https://doi.org/10.5006/1.3577363.
[16] T.S. Ellis, F.E. Karasz, Interaction of epoxy resins with water: the depression of glass transition temperature, Polymer 25 (1984) 664–669, https://doi.org/10.1016/0032-3861(84)90034-X.
[17] G.M. Foster, S. Ritchie, K.E. Evans, C. Lowe, Controlled relative humidity testing for the characterisation of the brittle-tough and glass transition temperatures of coil coating paint films, Prog. Org. Coat. 51 (2004) 244–249, https://doi.org/10.1016/j.porgcoat.2004.08.002.
[18] G.K. Van Der Wel, O.C.G. Adan, Moisture in organic coatings—a review, Prog. Org. Coat. 37 (1999) 1–14, https://doi.org/10.1016/S0300-9440(99)00058-2.
[19] T. Nguyen, J. Martin, E. Byrd, Relating laboratory and outdoor exposure of coatings: IV. Mode and mechanism for hydrolytic degradation of acrylic-melamine coatings exposed to water vapor in the absence of UV light, J. Coat. Technol. Res. 75 (2003) 37–50, https://doi.org/10.1007/BF02720521.
[20] M.A.J. Batista, R.P. Moraes, J.C.S. Barbosa, P.C. Oliveira, A.M. Santos, Effect of the polyester chemical structure on the stability of polyester–melamine coatings when exposed to accelerated weathering, Prog. Org. Coat. 71 (2011) 265–273, https://doi.org/10.1016/j.porgcoat.2011.03.009.
[21] J.L. Gerlock, H. Van Oene, D.R. Bauer, Nitroxide kinetics during photodegradation of acrylic/melamine coatings, Eur. Polym. J. 19 (1983) 11–18, https://doi.org/10.1016/0014-3057(83)90095-2.
[22] W.R. Zhang, S.J. Hinder, R. Smith, C. Lowe, J.F. Watts, An investigation of the effect of pigment on the degradation of a naturally weathered polyester coating, J. Coat. Technol. Res. 8 (2011) 329–342, https://doi.org/10.1007/s11998-010-9305-y.
[23] J. Mallégol, M. Poelman, M.-G. Olivier, Influence of UV weathering on corrosion resistance of prepainted steel, Prog. Org. Coat. 61 (2008) 126–135, https://doi.org/10.1016/j.porgcoat.2007.09.026.
[24] D. Santos, M.R. Costa, M.T. Santos, Performance of polyester and modified polyester coil coatings exposed in different environments with high UV radiation, Prog. Org. Coat. 58 (2007) 296–302, https://doi.org/10.1016/j.porgcoat.2007.01.006.
[25] V. Saarimaa, M. Virtanen, T. Laihinen, K. Laurila, P. Väisänen, Blistering of color coated steel: use of broad ion beam milling to examine degradation phenomena and coating defects, Surf. Coat. Technol. 448 (2022) 128913, https://doi.org/10.1016/j.surfcoat.2022.128913.
[26] D. Persson, G. Heydari, C. Edvinsson, P.E. Sundell, Depth-resolved FTIR focal plane array (FPA) spectroscopic imaging of the loss of melamine functionality of polyester melamine coating after accelerated and natural weathering, Polym. Test. 86 (2020) 106500, https://doi.org/10.1016/j.polymertesting.2020.106500.
[27] T. Hirayama, M.W. Urban, Distribution of melamine in melamine/polyester coatings; FT-IR spectroscopic studies, Prog. Org. Coat. 20 (1992) 81–96, https://doi.org/10.1016/0033-0655(92)85006-H.
[28] D.R. Bauer, L.M. Briggs, IR spectroscopic studies of degradation in cross-linked networks, ACS Symp. Ser. 243 (1984) 271–284, https://doi.org/10.1021/bk-1984-0243.ch016.
[29] A. Wärnheim, C. Edvinsson, P.-E. Sundell, G. Heydari, T. Deltin, D. Persson, Depth-resolved FTIR-ATR imaging studies of coating degradation during accelerated and natural weathering—influence of biobased reactive diluents in polyester melamine coil coating, ACS Omega 7 (2022) 23842–23850, https://doi.org/10.1021/acsomega.2c02523.

[30] L. Gonon, J. Mallegol, S. Commereuc, V. Verney, Step-scan FTIR and photoacoustic detection to assess depth profile of photooxidized polymer, Vib. Spectrosc. 26 (2001) 43–49, https://doi.org/10.1016/S0924-2031(01)00102-3.
[31] K.N.S. Adema, H. Makki, E.A.J.F. Peters, J. Laven, L.G.J. van der Ven, R.A.T.M. van Benthem, G. de With, Depth-resolved infrared microscopy and UV–VIS spectroscopy analysis of an artificially degraded polyester-urethane clearcoat, Polym. Degrad. Stab. 110 (2014) 422–434, https://doi.org/10.1016/j.polymdegradstab.2014.10.004.
[32] J.L. Gerlock, C.A. Smith, V.A. Cooper, T.G. Dusbiber, W.H. Weber, On the use of Fourier transform infrared spectroscopy and ultraviolet spectroscopy to assess the weathering performance of isolated clearcoats from different chemical families, Polym. Degrad. Stab. 62 (1998) 225–234, https://doi.org/10.1016/S0141-3910(97)00279-6.
[33] N. Caussé, P. Bonin, D. Thierry, N. LeBozec, A. Roggero, N. Pébère, Ageing processes of coil-coated materials: temperature-controlled electrochemical impedance analysis, Prog. Org. Coat. 183 (2023) 107682, https://doi.org/10.1016/j.porgcoat.2023.107682.
[34] P. Bonin, A. Roggero, N. Caussé, N. Pébère, D. Thierry, N. LeBozec, Impedance analysis of the barrier effect of coil-coated materials: water uptake and glass transition variations, Prog. Org. Coat. 153 (2021) 106163, https://doi.org/10.1016/j.porgcoat.2021.106163.
[35] N.S. Allen, M.J. Parker, C.J. Regan, R.B. McIntyre, W.A.E. Dunk, The durability of water-borne acrylic coatings, Polym. Degrad. Stab. 47 (1995) 117–127, https://doi.org/10.1016/0141-3910(94)00103-F.
[36] Y. Zhang, J. Maxted, A. Barber, C. Lowe, R. Smith, The durability of clear polyurethane coil coatings studied by FTIR peak fitting, Polym. Degrad. Stab. 98 (2013) 527–534, https://doi.org/10.1016/j.polymdegradstab.2012.12.003.
[37] D.R. Bauer, Melamine/formaldehyde crosslinkers: characterization, network formation and crosslink degradation, Prog. Org. Coat. 14 (1986) 193–218.
[38] N. Lesage, M. Vienne, S. Therias, P.O. Bussiere, Photoageing and durability of a polyester-melamine organic coating on steel: new insights into degradation mechanisms, Polym. Degrad. Stab. 229 (2024) 110944, https://doi.org/10.1016/j.polymdegradstab.2024.110944.
[39] M.E. Nichols, J.L. Gerlock, Rates of photooxidation induced crosslinking and chain scission in thermoset polymer coatings II. Effect of hindered amine light stabilizer and ultraviolet light absorber additives, Polym. Degrad. Stab. 69 (2000) 197–207, https://doi.org/10.1016/S0141-3910(00)00061-6.
[40] W.R. Zhang, T.T. Zhu, R. Smith, C. Lowe, A non-destructive study on the degradation of polymer coating I: step-scan photoacoustic FTIR and confocal Raman microscopy depth profiling, Polym. Test 31 (2012) 855–863, https://doi.org/10.1016/j.polymertesting.2012.07.002.
[41] A. Wärnheim, N. Kotov, I. Dobryden, R.T. Leggieri, C. Edvinsson, G. Heydari, P. E. Sundell, T. Deltin, C.M. Johnson, D. Persson, P.M. Claesson, Nanomechanical and nano-FTIR analysis of polyester coil coatings before and after artificial weathering experiments, Prog. Org. Coat. 190 (2024) 108355, https://doi.org/10.1016/j.porgcoat.2024.108355.
[42] W. Zhang, R. Smith, C. Lowe, Confocal Raman microscopy study of the melamine distribution in polyester–melamine coil coating, J. Coat. Technol. Res. 6 (2009) 315–328, https://doi.org/10.1007/s11998-008-9136-2.
[43] T. Greunz, C. Lowe, E. Bradt, S. Hild, B. Strauß, D. Stifter, A study on the depth distribution of melamine in polyester-melamine clear coats, Prog. Org. Coat. 115 (2018) 130–137, https://doi.org/10.1016/j.porgcoat.2017.11.014.
[44] G.P. Bierwagen, L. He, J. Li, L. Ellingson, D.E. Tallman, Studies of a new accelerated evaluation method for coating corrosion resistance — thermal cycling testing, Prog. Org. Coat. 39 (2000) 67–78, https://doi.org/10.1016/S0300-9440(00)00106-5.
[45] J.E.O. Mayne, The mechanism of the inhibition of the corrosion of iron and steel by means of paint, Off. Digest 24 (1952) 127.
[46] A. Roggero, N. Caussé, E. Dantras, L. Villareal, A. Santos, N. Pébère, Thermal activation of impedance measurements on an epoxy coating for the corrosion protection: II. electrochemical impedance spectroscopy study, Electrochim. Acta 305 (2019) 116–124, https://doi.org/10.1016/j.electacta.2019.03.007.
[47] F. Kremer, A. Schönhals. Broadband dielectric spectroscopy, Springer, 2003.
[48] E.D. Schachinger, B. Strauß, R. Braidt, A.W. Hassel, Electrochemical impedance spectroscopy on UV-aged polyester coatings: possibilities and limits of modeling water diffusion, Phys. Status Solidi A 217 (2020) 1901038, https://doi.org/10.1002/pssa.201901038.
[49] A.S. Castela, A.M. Sim, An impedance model for the estimation of water absorption in organic coatings. Part I: a linear dielectric mixture equation, Corr. Sci. 45 (2003) 1631–1646, https://doi.org/10.1016/S0010-938X(03)00014-3.
[50] A.S. Nguyen, N. Caussé, M. Musiani, M.E. Orazem, N. Pébère, B. Tribollet, V. Vivier, Determination of water uptake in organic coatings deposited on 2024 aluminium alloy: comparison between impedance measurements and gravimetry, Prog. Org. Coat. 112 (2017) 93–100, https://doi.org/10.1016/j.porgcoat.2017.07.004.
[51] A. Roggero, L. Villareal, N. Caussé, A. Santos, N. Pébère, Correlation between the physical structure of a commercially formulated epoxy paint and its electrochemical impedance response, Prog. Org. Coat. 146 (2020) 105729, https://doi.org/10.1016/j.porgcoat.2020.105729.
[52] D.M. Brasher, A.H. Kingsbury, Electrical measurements in the study of immersed paint coatings on metal. I. Comparison between capacitance and gravimetric methods of estimating water-uptake, J. Appl. Chem. 4 (1954) 62–72, https://doi.org/10.1002/JCTB.5010040202.
[53] J. Crank, Non-Fickian Diffusion in the Mathematics of Diffusion, Oxford University Press, 1995.
[54] F. Bellucci, L. Nicodemo, Water transport in organic coatings, Corrosion 49 (1993) 235–247, https://doi.org/10.5006/1.3316044.
[55] E.P.M. van Westing, G.M. Ferrari, J.H.W. de Wit, The determination of coating performance with impedance measurements—II. Water uptake of coatings, Corros. Sci. 36 (1994) 957–977, https://doi.org/10.1016/0010-938X(94)90197-X.
[56] A. Roggero, N. Caussé, E. Dantras, L. Villareal, A. Santos, N. Pébère, Thermal activation of impedance measurements on an epoxy coating for the corrosion protection: I. Dielectric spectroscopy response in the dry state, Electrochim. Acta 303 (2019) 239–245, https://doi.org/10.1016/j.electacta.2019.02.035.
[57] C. Perez, A. Collazo, M. Izquierdo, P. Merino, X.R. Novoa, Characterization of the barrier properties of different paint systems: part II. Non-ideal diffusion and water uptake kinetics, Prog. Org. Coat 37 (1999) 169–177, https://doi.org/10.1016/S0300-9440(99)00073-9.